Enrichment of neurodegenerative microglia signature in brain-derived extracellular vesicles isolated from Alzheimer's disease mouse model

Satoshi Muraoka[1], Mark P. Jedrychowski[2], Naotoshi Iwahara[1], Mohammad Abdullah[1], Kristen D. Onos[3], Kelly J. Keezer[3], Jianqiao Hu[1], Seiko Ikezu[1], Gareth R. Howell[3], Steven P. Gygi[2], Tsuneya Ikezu[1,4,5*]

[1]Department of Pharmacology & Experimental Therapeutics, Boston University School of Medicine, Boston, MA, USA; smuraoka@bu.edu (S.M.); niwahara@bu.edu (N.I.); moab@bu.edu (M.A.); lawrenhu@bu.edu (J.H.); sikezu@bu.edu (S.I.)

[2]Department of Cell Biology, Harvard Medical School, Boston, MA, USA; Mark_Jedrychowski@hms.harvard.edu (M.P.J.); steven_gygi@hms.harvard.edu (S.P.G.)

[3]The Jackson Laboratory, Bar Harbor, Maine, ME, USA; Kristen.Onos@jax.org (K.O.); Kelly.keezer@jax.org (K.J.K); Gareth.Howell@jax.org (G.H.)

[4]Department of Neurology, Alzheimer's Disease Center, Boston University School of Medicine, Boston, MA, USA

[5]Center for Systems Neuroscience, Boston University, Boston, MA, USA

[#]**Correspondence author:** Tsuneya Ikezu, MD, PhD

Boston University School of Medicine, 72 East Concord St, L-606B, Boston, MA 02118, USA. Email: tikezu@bu.edu Phone: 617-358-9575 Fax: 617-358-9574

Running title: Protein profiling of CAST.*APP/PS1* mouse brain-derived EVs

25 **Abbreviations**

26 Aβ: Amyloid beta peptide

27 AD: Alzheimer's disease

28 ANXA5: Annexin-5

29 APOE: Apolipoprotein E

30 APP: Amyloid precursor protein

31 BCA: Bicinchoninic acid

32 CNS: Central nervous system

33 CYC1: Cytochrome C

34 DAM/MGnD: disease-associated / neurodegenerative microglia

35 DAVID: Database for annotation, visualization, and integrated discovery

36 DEP: Differentially expressed proteins

37 EVs: Extracellular vesicles

38 FAD: Early-onset / familial AD

39 GM130: 130 kDa cis-Golgi matrix protein

40 HO: Homeostatic microglia

41 ITGAX: Integrin alpha-x

42 LOAD: Sporadic / late-onset AD

43 MS: Mass spectrometry

44 MVBs: Multivesicular bodies

45 NFT: Neurofibrillary tangles

46 NTA: Nanoparticle tracking analysis

47 PS1: Presenilin-1

48 TEM: Transmission electron microscopy

49 TSG101: Tumor susceptibility gene 101 protein

50 UC: Ultracentrifugation

51 TMT: Tandem mass tag

52

53

54

55

56

57

58

59

60

61

62

63

64

65

66

67

68

69

70

Abstract

Extracellular vesicles (EVs) are secreted by any neuronal cells in the central nervous system (CNS) for molecular clearance, cellular communications and disease spread in multiple neurodegenerative diseases, including Alzheimer's disease (AD), although their exact molecular mechanism is poorly understood. We hypothesize that high-resolution proteomic profiling of EVs separated from animal models of AD would determine the composition of EV contents and their cellular origin. Here, we examined recently developed transgenic mice (CAST.*APP/PS1*), which express familial AD-linked mutations of amyloid precursor protein (*APP*) and presenilin-1 (*PS1*) in the CAST/EiJ mouse strain and develop hippocampal neurodegeneration. Quantitative proteomics analysis of EVs separated from CAST.*APP/PS1* and age-matched control mice by tandem mass tag-mass spectrometry identified a total of 3,444 unique proteins, which are enriched in neuron, astrocyte, oligodendrocyte and microglia-specific molecules. CAST.*APP/PS1*-derived EVs show significant enrichment of Psen1, APP, Itgax, and reduction of Wdr61, Pmpca, Aldh1a2, Calu, Anp32b, Actn4 and Ndufv2 compared to WT-derived EVs, suggesting the involvement of Aβ-processing complex and disease-associated / neurodegenerative microglia (DAM/MGnD) in EV secretion. In addition, Itgax and Apoe, the DAM/MGnD markers, in EV show a positive correlation with *Itgax* and *Apoe* mRNA expression from brain tissue in CAST.*APP/PS1* mice. These datasets indicate the significant contribution of Aβ plaque and neurodegeneration-induced DAM/MGnD microglia for EV secretion in CAST.*APP/PS1* mice and shed light on understanding the AD pathogenesis.

Keywords: Alzheimer's disease, amyloid-β peptide, amyloid precursor protein, apolipoprotein E, extracellular vesicles, integrin, microglia, presenilin-1, proteome

94 **Introduction**

95 Alzheimer's disease (AD) is a progressive neurodegenerative disorder and the most common
96 forms of adult dementia affecting 50 million people worldwide (1). The neuropathology of AD is
97 characterized by extracellular deposition of amyloid-β (Aβ) plaques, which are processed by
98 amyloid precursor protein (APP) and presenilin-1 (PS1)-dependent gamma secretase complex,
99 and intraneuronal accumulation of neurofibrillary tangles (NFTs), which are consisted with
100 hyperphosphorylated microtubule-associated protein tau (2-4). There are two form of AD, early-
101 onset / familial AD (FAD) and sporadic / late-onset AD (LOAD) (5, 6). FAD is mostly caused
102 by mutations in *APP* and *PSEN1* and *PSEN2* (7). The FAD mouse models expressing FAD-
103 linked mutation of *APP, PSEN1* or both, have been extensively used to understand the
104 pathophysiology of Aβ deposition although most of them do not develop neurodegeneration (8-
105 10). Onos *et al.* have recently reported a comprehensive assessment of the transgene expression
106 of FAD-linked mutation of *APP* and *PSEN1* in different genetic backgrounds including B6,
107 WSB/EiJ, PWK/PhJ, and CAST/EiJ to establish more clinically-relevant AD mouse models (11).
108 The study showed that CAST.*APP/PS1* line develops reduction in the number of hippocampal
109 pyramidal neurons and robust neuroinflammatory response than previous models (11), which
110 would be more suitable for the assessment of Aβ deposition-induced inflammatory reaction and
111 neuronal cell loss.

112 Extracellular vesicles (EVs), including exosomes (50-150nm), ectosomes/microvesicles
113 (150-1000nm), and apoptotic bodies (1000-5000nm) are released from almost any neuronal cells
114 (12-14). These EVs contain proteins, mRNA, non-coding RNAs (such as microRNA) and lipids,
115 can transfer these molecules from cells to cells, and can be transported to biofluids, such as and
116 cerebrospinal fluid and blood. In the central nervous system (CNS), brain-derived EVs contain

117 multiple AD-associated proteins such as Aβ, α-synuclein, APP, cyclin-dependent kinase 5,
118 PSEN1, and tau, and play important roles in Aβ deposition and tauopathy (15-20). Moreover, it
119 has been reported that inhibition of EV synthesis reduced Aβ plaque deposition in the mouse
120 model of AD, and stimulation of EV secretion increased intracellular transfer of prion protein in
121 AD mouse models (16, 17). EVs are involved in the extracellular enzymatic degradation of Aβ
122 and promote both Aβ aggregation and clearance by microglia (18, 19), although their exact
123 molecular mechanism is poorly understood. We hypothesize that high-resolution proteomic
124 profiling of EVs separated from animal models of AD would determine the composition of EV
125 contents and their cellular origin. Here we provide the quantitative proteomics profiling of EVs
126 separated from CAST.*APP/PS1* transgenic mouse brain tissue and show brain-derived EV
127 molecules altered during early-onset AD.
128

129 **Materials and methods**

130 **CAST.-*APP/PS1* transgenic mouse model**

131 The CAST.-*APP/PS1* transgenic mouse line, which expresses human APP^{swe} and $PS1^{de9}$, was
132 created in the Howell lab colony at The Jackson Laboratory by backcrossing for at least seven
133 generations the *APP/PS1* transgenes from C57BL/6J (B6) to CAST (11). Brain samples
134 (forebrain and hindbrain) were extracted from 6 female CAST.*APP/PS1* and 6 female CAST
135 (WT) littermate control mice at 8 months of age. Mice were anesthetized with ketamine/xylazine
136 prior to tissue harvest.

137 **Brain tissue homogenates**

138 Frozen whole brain tissue was chopped on ice using a razor blade (# 12-640 Fischer Scientific)
139 to generate approximately 0.5 mm-wide pieces, and homogenized by a sonicator. The
140 homogenized tissue was lyzed using Guanidine Hydrochloride (# 50950-250G Sigma).

141 **Separation of EVs from mouse brain tissue**

142 Brain tissue (0.4 g per sample) was processed for EV extraction based on our reported method
143 with modifications. Briefly, frozen whole brain tissue was chopped on ice using a razor blade (#
144 12-640 Fischer Scientific) to generate approximately 0.5 mm-wide pieces. The sections were
145 transferred to 3mL of Hibernate E solution (# A1247601 Gibco) containing 20 U of papain (#
146 LK003178 Worthington-biochemical corporation) in Earle's Balanced Salt Solution (EBSS) (#
147 14155063 Gibco) and then incubated at 37°C for 15 min by stirring once every 5 min. After the
148 incubation, the samples were placed on ice, and added with 6 mL of ice-cold Hibernate E
149 solution supplemented with Halt™ Protease and Phosphatase Inhibitor Cocktails (# PI78443
150 Fisher scientific). The samples were gently homogenized (20 strokes) with a glass-Teflon
151 homogenizer (# 89026-384 VWR), and filtered with 40-µm mesh filter (# 22-363-547 Fisher
152 scientific), followed by centrifugation at 300 × *g* for 10 min at 4°C (# 5720R Eppendorf). The
153 supernatant was transferred to a new 15-mL polypropylene tube and centrifuged at 2,000 × *g* for
154 10 min at 4°C (# 5720R Eppendorf). The supernatant was transferred to a 30-mL conical tube
155 and centrifuged at 10,000 × *g* for 10 min at 4°C (#5424R Eppendorf). The supernatant filtered
156 through a 0.22-µm polyethersulfone membrane filter (# SLGP033RS EMD Millipore) into new a
157 polyallomer ultracentrifuge tube with 13.2-mL capacity (# 331372 Beckman Coulter), diluted
158 with double-filtered phosphate-buffered saline (dfPBS) with 0.22-µm polyethersulfone
159 membrane filter to 12 mL, and centrifuged at 140,000 × *g* for 70 min at 4°C (# Optima-XE
160 SW41 Beckman Coulter). The pellet was resuspended in 2 mL of 0.475M of sucrose solution (#

161 S5-3 Fisher science) in dfPBS. The sucrose step gradient was created in dfPBS with six 2-mL
162 steps starting from 2.0M to 1.5M, 1.0M, 0.825M, 0.65M, and 0.475M (containing the
163 resuspended pellet) in a polyallomer ultracentrifuge tube. The gradient was centrifuged at
164 200,000 × *g* for 20 h at 4°C (35,000 rpm with # Optima-XE SW41 Beckman Coulter). The
165 gradient was collected in 2-mL fractions, except for the first and last fractions, which were 1 mL
166 each. The interphases between the second (0.65M) and third (0.825M) steps correspond to
167 fraction "V" and the third and fourth steps corresponded to fraction "VI" have a buoyant density
168 of 1.10 - 1.12 and 1.12 - 1.15 g/cm^3, respectively, and enriched in EVs. The V and VI fractions
169 were diluted to a total volume of 12 mL with dfPBS and centrifuged at 140,000 × *g* for 70 min at
170 4°C (# Optima-XE SW41 Beckman Coulter), and each pellet were resuspend with 30 µl of
171 dfPBS. The fraction V and VI fractions were mixed as an EV-enriched sample.

172 **Protein concentrations**

173 The bicinchoninic acid (BCA) assay was used to determine protein concentration for each
174 sample using BCA protein assay kit (# 23225 Pierce) as previously described (21). EVs were
175 diluted 1:10 before loading into the assay, and a 1:8 ratio of sample to reaction components was
176 used. All assays were allowed to incubate at 37°C for 30 min before protein concentration was
177 read in at 562 nm (SynergyMix, Biotek).

178 **Nanoparticle Tracking Analysis (NTA)**

179 All samples were diluted in dfPBS at least 1:8000 to get particles within the target reading range
180 for the Nanosight 300 machine (Malvern Panalytical Inc), which is 10-100 particles per frame.
181 Using a manual injection system, four 60-s videos were taken for each sample at 21°C. Analysis
182 of particle counts was carried out in the Nanosight NTA 3.2 software (Malvern Panalytical Inc)
183 with a detection threshold of 5.

184 **Transmission electron microscopy (TEM)**

185 The EV separated from *APP/PS1* and control mouse brain tissue were analyzed by TEM. The
186 EV sample (5µl) was adsorbed for 1 min to a carbon-coated mesh grid (# CF400-CU, Electron
187 Microscopy Sciences) that had been made hydrophilic by a 20-s exposure to a glow discharge
188 (25 mA). Excess liquid was removed with a filter paper (# 1 Whatman). The grid was then
189 floated briefly on a drop of water (to wash away phosphate or salt), blotted on a filer paper, and
190 then stained with 0.75% uranyl formate (# 22451 Electron Microscopy Sciences) for 30 s. After
191 removing the excess uranyl formate, the grids were examined, and random fields were
192 photographed using a JEOL 1200EX TEM with an AMT 2k CCD camera at the Electron
193 Microscopy Facility, Harvard Medical School, Boston, MA.

194 **Western blotting**

195 EV samples and brain tissue homogenate samples were run in a 4% to 20% gradient gel (#
196 4561093 Bio-Rad) and electro-transferred to Immobilon-P membrane, PVDF 0.45-µm (#
197 10344661 Fisher scientific). The membrane was blocked in freshly prepared 5% BSA diluted in
198 TBS before being immunoblotted with specific primary antibodies (CD81; #EXOAB-CD81A-1
199 System Biosciences, GM130; #610822 Becton Dickinson, Cytochrome C; #11940T Cell
200 Signaling Technology, ANXA5, ItgaX; #14-011485 eBioscience) or HRP-labeled primary
201 antibodies (TSG101; # SC-7964 Santa Cruz Biotechnology). The membrane was incubated with
202 HRP-labeled secondary antibodies (Santa Cruz Biotechnology) and scanned using the C300
203 digital chemiluminescent imager (Azure Biosystems).

204 **High-Resolution Liquid Chromatography-Tandem Mass-tag Mass spectrometry**

205 **SDS-PAGE and In-gel digestion**

206 Ice-cold 100% (w / v) trichloroacetic acid (TCA) (# T6399 Sigma-Aldrich) was added to the
207 separated EV fraction to a final concentration of 20% of TCA, then the mixed sample was
208 incubated for 30 min on ice and was centrifuged at 15,000 g for 20 min at 4°C. The pellet was
209 then washed twice with ice-cold acetone (# 179124 Sigma-Aldrich). After drying, the pellet was
210 resuspended in Laemmli sample buffer (# 1610747 Bio-Rad) with 5 mM dithiothreitol (# 43815
211 Sigma-Aldrich), reduced for 20 min at 65°C, and alkylated with 15 mM iodoacetamide (# I1149
212 Sigma-Aldrich) for 20 min at room temperature in the dark. Subsequently, the samples were run
213 in a 4% to 20% gradient gel (# 4561096 Bio-Rad) until the dye front was 10 mm from the top of
214 the gel. The gels were washed twice with distilled water, fixed with 100% Methanol, and stained
215 with GelCode Blue Stain Reagent (# 24590 Thermo Fisher Scientific) for 16 hrs. Each lane was
216 then individually removed from the gel. Gel pieces were then transferred to 1.5 mL tubes and
217 destained twice using 50% acetonitrile (J. T. Baker, USA) in 25 mM HEPES (pH 8.8) at 22°C,
218 for 15 min with shaking, and dehydrated with 100% acetonitrile for additional 10 min with
219 shaking, for a total of three times. The destained gel piece was dried up using SpeedVac
220 Concentrators (Thermo Fisher Scientific). The gel pieces were digested with proteomic grade
221 trypsin (# 03708985 Roche, USA) in 25 mM HEPES overnight at 37°C. The digested peptide
222 was extracted with 70% acetonitrile /1% formic acid, and were removed the gel by Ultrafree-MC
223 Centrifugal Filter (# UFC30L Millipore USA). The digested peptides were reconstituted in 25 µL
224 of 200 mM EPPS (pH 8.0) and vortexed for 5 min.

225 **Peptide labeling with TMT 16-plex isobaric labeling Kit**

226 Tandem mass tag (TMT) labeling was performed according to manufacturer's instructions (#
227 A44520 Thermo Fisher Scientific). In brief, 4 µL of TMT Label reagent (20 ng/µL) was added to
228 the digested peptides in 30 µL of 200 mM HEPPS (4-(2-Hydroxyethyl)-1-

229 piperazinepropanesulfonic acid), pH8.0. After incubation at room temperature for 1 h, the
230 reaction was quenched with 2 μL of 5% hydroxylamine in water for 15min. The TMT-labeled
231 peptide samples were pooled at a 1:1 ratio across ten samples. The combined sample was added
232 to 100 μL of 20% formic acid, 2 mL of 1% formic acid, desalted via StageTip, dried by vacuum
233 centrifugation, and resuspended in 20 μL of 5% acetonitrile and 5% formic acid for nano liquid
234 chromatography and tandem mass-spectrometry (Nano LC-MS/MS/MS).

235 **Nano-Liquid Chromatography and Tandem Mass-tag Spectrometry (LC-MS/MS/MS)**

236 Nano LC–MS/MS/MS analysis was conducted using an LTQ-Orbitrap Fusion Lumos mass
237 spectrometer (Thermo Fisher Scientific, USA) equipped with a Proxeon EASY-nano LC 1200
238 liquid chromatography pump (Thermo Fisher Scientific, San Jose, CA). Peptides were separated
239 on a 100 μm inner diameter microcapillary column packed with 35-cm long Accucore150 resin
240 (2.6 μm, 150 Å, Thermo Fisher Scientific). We loaded 4 μL onto the column and separation was
241 achieved using a 180 min gradient of 8 to 23% acetonitrile in 0.125% formic acid at a flow rate
242 of ~550 nL/min. The analysis used an MS^3 based TMT method, which has been shown to reduce
243 ion interference. The scan sequence began with an MS1 spectrum (Orbitrap; resolution 120,000;
244 mass range 400-1400m/z; automatic gain control (AGC) target 5×10^5; maximum injection time
245 100ms). Precursors for MS^2/MS^3 analysis were selected using a Top10 method. MS2 analysis
246 consisted of collision-induced dissociation (quadrupole ion trap; AGC 2×10^4; normalized
247 collision energy (NCE) 35; maximum injection time 150ms). Following acquisition of each MS^2
248 spectrum, we collected an MS^3 spectrum using our recently described method in which multiple
249 MS^2 fragment ions were captured in the MS^3 precursor population using isolation waveforms
250 with multiple frequency notches (22). MS^3 precursors were fragmented by high-energy collision-

251 induced dissociation (HCD) and analyzed using the Orbitrap (NCE 65; AGC 1×10^5; maximum
252 injection time 150ms, resolution was 50,000 at 200Th).

253 **Mass-spectrometry data analysis**

254 A compendium of in-house developed software was used to convert mass spectrometric data
255 (Raw file) to the mzXML format, as well as to correct monoisotopic m/z measurements (23).
256 Database searching included all entries from the *Mus musculus* with human APP and PS1
257 UniProt database (ver. October 2018). This database was concatenated with one composed of all
258 protein sequences in the reversed order. Searches were performed using a 50ppm precursor ion
259 tolerance for total protein level profiling (22). The product ion tolerance was set to 0.9 Da, which
260 was chosen to maximize sensitivity in conjunction with SEQUEST searches and linear
261 discriminant analysis. TMT tags on lysine residues and peptide N termini (+229.163 Da) and
262 carbamidomethylation of cysteine residues (+57.021 Da) were set as static modifications, while
263 oxidation of methionine residues (+15.995 Da) was set as a variable modification. Peptide-
264 spectrum matches (PSMs) were adjusted to a 1% false discovery rate (FDR). Filtering was
265 performed using an in-house linear discrimination analysis (LDA) method to create one
266 combined filter parameter from the following peptide ion and MS^2 spectra metrics: SEQUEST
267 parameters XCorr and ΔCn, peptide ion mass accuracy and charge state, in-solution charge of
268 peptide, peptide length, and mis-cleavages. Linear discrimination scores were used to assign
269 probabilities to each MS^2 spectrum for being assigned correctly, and these probabilities were
270 further used to filter the dataset with an MS^2 spectra assignment FDR of smaller than 1% at the
271 protein level (24). For TMT-based reporter ion quantitation, we extracted the summed signal-to-
272 noise (S/N) ratio for each TMT channel and found the closest matching centroid to the expected
273 mass of the TMT reporter ion. PSMs were identified, quantified, and collapsed to a 1% peptide

274 FDR and then collapsed further to a final protein-level FDR of 1%. Moreover, protein assembly
275 was guided by principles of parsimony to produce the smallest set of proteins necessary to
276 account for all observed peptides. Proteins were quantified by summing reporter ion counts
277 across all matching PSMs. PSMs with poor quality, MS^3 spectra with more than eight TMT
278 reporter ion channels missing, MS^3 spectra with TMT reporter summed signal-to-noise ratio less
279 than 100, or no MS^3 spectra were excluded from quantification (25). The mass spectrometry
280 proteomics data have been deposited to the ProteomeXchange Consortium via the PRIDE partner
281 repository (26) with the dataset identifier PXD022349 (Username:
282 reviewer_pxd022349@ebi.ac.uk, pa$$word: 4ot9rIHF). Protein quantitation values were
283 exported for further analysis in Microsoft Excel or Prism8. Each reporter ion channel was
284 summed across all quantified proteins.

285 **Experimental design and statistical analysis**

286 EVs were isolated from brain tissue of 6 female CAST.*APP/PS1* and 6 female CAST (WT)
287 littermate control mice at 8 months of age. Statistical analysis was conducted using Prism 8
288 (GraphPad, Inc.). Between group comparisons were analyzed by Welch's t-test. The Gene
289 Ontology of identified proteins were elucidated by the Database for Annotation, Visualization
290 and Integrated Discovery (DAVID) Bioinformatics Resources 6.8. The venn diagram and
291 heatmap analysis were generated using Venny_2.1 (http://bioinfogp.cnb.csic.es/tools/venny/) and
292 ClustVis (https://biit.cs.ut.ee/clustvis/).
293

294 **Results**

295 **Biochemical and morphological characterization of EVs separated from brain tissue**

296 We separated EVs from mouse brain tissues by ultracentrifugation and sucrose gradient
297 ultracentrifugation as previously described (21). To check the purity of the EV preparation from
298 mouse brain tissues, the EV fractions were analyzed for their size and number by NTA. The EV
299 fractions were enriched the particle of small size (median 122 nm) compared to brain
300 homogenate (median 165 nm, **Figure 1A**). The particles per protein were 2.08×10^7 [particles /
301 μg] in brain homogenate and 1.40×10^9 [particles / μg] in separated EV fraction (**Figure 1B**),
302 showing significant enrichment ($p < 0.001$). The EV markers such as Tumor susceptibility gene
303 101 protein (TSG101) and CD81 were clearly represented in EV fractions, whereas
304 contamination markers such as 130 kDa cis-Golgi matrix protein (GM130) and cytochrome C
305 (CYC1) in MISEV2018 guidelines (12) were absent in the EV fraction (**Figure 1C**). The
306 separated EVs were examined by transmission electron microscopy (TEM), which shows cap-
307 shaped morphology as commonly seen separated EVs (**Figure 1D**). These data demonstrate the
308 successful enrichment of EV fraction from mouse brain tissues.

309 **Proteomic profiling of EVs from CAST.*APP/PS1* and WT mouse brain tissue**

310 The median diameter of separated EVs was 120 nm for WT and 112 nm for *APP/PS1* groups,
311 and the particle counts were 7.03×10^{11} particles for WT and 1.38×10^{12} particles for *APP/PS1*
312 groups (**Figure 2A**). There were no significantly difference in these parameters between WT and
313 *APP/PS1* groups (Diameter: $p = 0.4848$, particle counts: $p = 0.0649$). We next analyzed the
314 protein profiles of EVs separated from *APP/PS1* and WT mouse brain tissues by LC-MS/MS/MS
315 using TMT-based labeling (27). We identified a total of 3444 unique proteins **(Supplementary**
316 **Table S1 and S2)**. The identified proteins were compared with the top 100 EV proteins from the
317 ExoCarta database (28). The Venn diagram represents 90 of the top 100 EV proteins commonly
318 found in the mouse brain-derived EVs **(Figure 2B)**. We analyzed the proteomic dataset using

319 Database for Annotation, Visualization, and Integrated Discovery (DAVID Gene Ontology
320 (GO)) (29, 30). The identified proteins show significantly enrichment of extracellular exosome
321 by 'cellular component', and transport and protein-binding molecules by 'Biological process'
322 and 'Molecular function', respectively (**Figure 2C**). The KEGG pathway analysis showed
323 enrichment of endocytosis and glutamatergic synapse molecules, which are related to microglia
324 and neuronal functions. The EV proteins were mostly annotated brain, brain cortex and
325 hippocampus by Tissue ontology as expected **(Figure 2C)**. Taken together, these results show
326 successful enrichment of proteins specific to EVs, cadherin/protein binding molecules, neuronal
327 /glial functions and brain tissues in separated EV samples.

328 **Neural cell-type specific proteins of EVs derived from mouse brain tissue**

329 We next examined the enrichment of neural cell-type specific molecules in the EV proteomic
330 dataset using the proteomic dataset of neural cells, such as neurons, astrocytes, microglia and
331 oligodendrocytes separated from mouse brain tissues by a bio-panning method as a reference
332 (31). The identified neural cell-type specific markers (155 total) are 43.9 % (68) neurons, 5.8%
333 (9) microglia, 27.1% (42) astrocytes and 23.2% (36) oligodendrocytes **(Figure 3A)**. We
334 examined the changes in the expression of these cell type-specific markers in EVs separated
335 from *APP/PS1* and WT groups. The neuron-specific molecules downregulated in *APP/PS1*
336 compared to WT include Pclo (Piccolo), Add2 (Beta-adducin), L1cam (Neural cell adhesion
337 molecule L1), Calb2 (Calretinin) and Calb1 (Calbindin), while upregulated molecules include
338 Camkv (CaM kinase-like vesicle-associated protein), Gprin1 (G protein-regulated inducer of
339 neurite outgrowth 1), Ngef (Ephexin-1), and Fxyd6 (FXYD domain-containing ion transport
340 regulator 6) (**Figure 3B**). The astrocyte-specific molecules downregulated in *APP/PS1* compared
341 to WT include Aldh1a2 (Retinal dehydrogenase 2), Nid1 (Nidogen-1), Lamb2 (Laminin subunit

342 beta-2) and Cbs (Cystathionine beta-synthase), while upregulated molecules include Sorbs1
343 (Sorbin and SH3 domain-containing protein 1), Fmn2 (Formin-2) and Pacsin3 (Protein kinase C
344 and casein kinase II substrate protein 3). The oligodendrocyte-specific molecules downregulated
345 in *APP/PS1* compared to WT include P4ha1 (Prolyl 4-hydroxylase subunit alpha-1), Mog
346 (Myelin-oligodendrocyte glycoprotein), Tnr (Tenascin-R) and Hmgcs1 (Hydroxymethylglutaryl-
347 CoA synthase, cytoplasmic), while upregulated molecules include Col1a1 (Collagen alpha-1(I)
348 chain), Pde9a (High affinity cGMP-specific 3',5'-cyclic phosphodiesterase 9A) and Cnp (C-type
349 natriuretic peptide). There are limited changes in the microglia-specific molecules identified by
350 the previous proteomic study. To compensate the information, we have used the microglia-
351 specific gene signature identified from microglia separated from another *APP/PS1* mouse models
352 (32-34), namely disease-associated/neurodegenerative microglia (DAM/MGnD) and homeostatic
353 microglia (HO). We identified DAM/MGnD-specific molecules, especially integrin alpha-x
354 (Itgax) and apolipoprotein E (Apoe) upregulated in EVs from *APP/PS1* compared to WT group
355 as determined by the scattered plot analysis of Log_2 fold changes of EV proteomic dataset and
356 the microglia gene expression profile (**Figure 3C**). These data indicate global changes in the
357 contribution of EV production in different neural cell types, suggesting their potential application
358 in monitoring the disease progression and understanding the pathobiology.

359 **Comparison of *APP/PS1* and WT mouse brain-derived EV proteins by TMT-labeling**
360 **proteomics analysis**

361 We analyzed the fold change and *p*-values of proteins by Volcano plot, which shows that 3
362 proteins were significantly upregulated ($p < 0.05$, $Log_2FC > 0.585$ or < -0.5585) , while 7
363 proteins were significantly down-regulated in *APP/PS1* compared to the WT **(Figure 4A)**. The
364 three significantly upregulated molecules are Psen1, App and Itgax (**Figure 4B**). Among them,

365 Psen1 and App are likely due to their transgene expression in *APP/PS1* mice, thus Itgax
366 (CD11c), which is the most representative marker of DAM/MGnD, is the only endogenous
367 molecule significantly upregulated in the separated EVs from *APP/PS1* mouse brain. The seven
368 significantly downregulated molecules are WD repeat-containing protein 61 (Wdr61),
369 Mitochondrial-processing peptidase subunit alpha (Pmpca), Retinal dehydrogenase 2 (Aldh1a2,
370 also astrocyte-specific marker), Calumenin (Calu), Acidic leucine-rich nuclear phosphoprotein
371 32 family member B (Anp32b), Alpha-actinin-4 (Actn4), and NADH dehydrogenase
372 flavoprotein 2 (Ndufv2) **(Figure 4C)**. The 46 significantly differentially expressed proteins
373 (DEPs, $p < 0.05$) are displayed in a heatmap, showing two clusters either upregulated or
374 downregulated in *APP/PS1* compared to WT group **(Figure 4D)**. The upregulated proteins
375 include Anxa5 (Annexin-5), which specifically binds to the phosphatidylserine expressed on
376 dying cells (35). We recently reported ANXA5 as the most upregulated molecules in AD brain-
377 derived EVs compared to healthy control group (20). We also confirmed the expression of
378 ANXA5 by immunoblotting of EVs separated from *APP/PS1* and WT mouse brains
379 **(Supplementary Figure. S1)**. We compared the ratio of mRNA levels in *APP/PS1* mouse brain
380 tissues over WT controls, which was published (11) and the ratio protein levels EVs separated
381 from *APP/PS1* mouse brains over WT controls in this study by a scattered plot (**Figure 4E**). The
382 Itgax protein show highly positive correlation with Itgax mRNA level ($\log_2$ mRNA expression
383 ratio; 3.77, $\log_2$ EV protein expression ratio; 1.44). These data demonstrate that DAM/MGnD
384 induction in *APP/PS1* mouse brain, as determined by Itgax expression, may contribute to the
385 enhanced EV production by microglia, which is shown in the upregulation of Itgax in *APP/PS1*
386 mouse brain-derived EVs. The ItgaX protein was upregulated in EVs separated from *APP/PS1*
387 mouse brains using immunoblotting **(Figure 4F)**.

388

389 **Discussion**

390 In the present study, we separated EVs from brain tissue of CAST.*APP/PS1* transgenic mice and
391 age-matched CAST WT littermates. The EV samples were biophysically and morphologically
392 characterized and subjected TMT-labeled high-resolution quantitative proteomic profiling by
393 Nano LC-MS/MS/MS. A total of 3,444 unique proteins from brain-derived EVs, were found to be
394 enriched as extracellular exosomes molecules. The identified EV proteins were enriched in neural
395 cell type and DAM/MGnD -specific molecules in CAST.*APP/PS1* compared to WT group. Itgax,
396 the DAM/MGnD marker, was significantly upregulated in EVs from CAST.*APP/PS1* compared
397 to WT mouse brains. In addition, the significantly increased level of ANXA5 in the
398 CAST.*APP/PS1* group, which was also increased in AD brain-derived EVs, was confirmed by
399 western blot.

400 The protein levels of APP and Psen1 were also significantly upregulated in CAST.*APP/PS1*
401 brain-derived EVs compare to WT. The peptides of APP identified in both groups by Nano-LC-
402 MS/MS, which covered 14.5% of APP, including the corresponding amyloid-β peptide region
403 **(Supplementary Figure S2)**. The quantification value of identified peptides, which contain
404 amyloid beta peptide and C-terminal peptide showed to upregulate 1.5 - 2.0 folds in
405 CAST.*APP/PS1* compared to WT in **Supplementary Table S3**. The EV in CAST.*APP/PS1*,
406 therefore, may contain amyloid-β peptide, full-length APP and cleaved C-terminal APP. Our
407 attempt to detect these molecules by ELISA was unsuccessful due to the scarcity of the target
408 molecules (data not shown).

409 Itgax is a well-established integrin and form complex with Integrin beta2 (Itgb2/CD18) as
410 inactivated-C3b receptor 4 (complement receptor 4) (36). The expression levels of Itgax is

411 specifically increased in DAM/MGnD microglia separated from aged *APP/PS1* mice (37). In
412 addition, we have recently shown that amyloid plaque-associated Mac2^{+} DAM/MGnD microglia
413 hyper-secrete EVs to extracellular regions in *App*$^{NL\text{-}G\text{-}F}$ knockin mouse model, demonstrating that
414 DAM/MGnD plays a key role in EV secretion in AD mouse brains (38).

415 We compare the EV proteomics data to human AD brain-derived EV proteomics data (20),
416 the 380 proteins were common between CAST.*APP/PS1* brain-derived EVs and human AD brain-
417 derived EVs **(Supplementary Figure S3)**. The APOE, CAMKV, ANXA5 and VGF showed a
418 similar correlation with these EVs, suggesting that Aβ deposition may be the major pathology for
419 the upregulation of these molecules in EVs.

420 The study has some limitation. The first is the limited amount of EVs that can be separated
421 from mouse brain (9.7 - 27.5 μg/whole brain). It is often difficult to detect proteins of interest
422 unless highly sensitive quantification method (such as digital ELISA) is available with the limited
423 amount of proteins. The second is the depth of identified neural cell type-specific molecules from
424 mouse brains that are publicly available. This is especially an issue for microglia-specific markers
425 in this study. This can be compensated by the dataset of cell type-specific gene expression analysis,
426 but these molecules still need to be validated by proteomic approaches. Another issue is the lack
427 of other neuropathology in *APP/PS1* mouse models, such as tau accumulation, cortical atrophy,
428 which may attribute to the difference in proteomic profiles of EVs separated from human and
429 mouse brain tissues. Further studies will be necessary to address these limitations by the use of
430 more robust and sensitive protein detection systems, development of more comprehensive dataset
431 for neural cell type-specific proteome, and application of animal models more closely
432 recapitulating AD progression in brain.

433 In summary, we have profiled a total of 3,444 proteins in EV samples separated from
434 CAST.*APP/PS1* and CAST WT mouse brain tissues at 8 months of age. *APP/PS1* mouse brain-
435 derived EVs are enriched in App, Psen1, Itgax and Anxa5, representing the amyloid pathology
436 progression, contribution of DAM/MGnD-derived EVs and apoptotic cell-detecting molecules: A
437 highly relevant molecular set for understanding the disease progression in *APP/PS1* mouse brains.
438

439 **Acknowledgment**
440 The authors thank M. Ericsson (Electron Microscopy Facility, Harvard Medical School) for
441 electron microscopic imaging services.
442

443 **Conflict of Interest**
444 The authors declare that the research was conducted in the absence of any commercial or
445 financial relationships that could be construed as a potential conflict of interest.
446

447 **Author Contributions**
448 S.M. and T.I. designed research; S.M., M.P.J., N.I., M.A., and K.O. performed research; S.M.,
449 M.P.J., N.I., J.H., and S.P.G. analyzed data; L.O., and G.H. provided brain sample; and S.M.,
450 and T.I. wrote the paper; S.M., W.P.J., N.I., M.A., S.I., and T.I. edited the paper.
451

452 **Funding**
453 This work is in part funded by Alzheimer's Association AARF-9550302678 (SM), Cure
454 Alzheimer's Fund (TI), NIH R01 AG066429 (TI), NIH RF1 AG054199 (TI), NIH R56

455 AG057469 (TI), NIH RF1 AG051496 (GRH), NIH RF1 AG055104 (GRH) and BU ADC P30
456 AG013846 (SI).

457

458 **References**

459 1. Selkoe, D. J., and Hardy, J. (2016) The amyloid hypothesis of Alzheimer's disease at
460 25 years. *EMBO Mol Med* 8, 595–608
461 2. Masters, C. L., Bateman, R., Blennow, K., Rowe, C. C., Sperling, R. A., and Cummings,
462 J. L. (2015) Alzheimer's disease. *Nat Rev Dis Primers* 1, 15056
463 3. Ittner, L. M., and Götz, J. (2011) Amyloid-β and tau--a toxic pas de deux in Alzheimer's
464 disease. *Nat. Rev. Neurosci.* 12, 65–72
465 4. Goedert, M. (2015) NEURODEGENERATION. Alzheimer“s and Parkinson”s diseases:
466 The prion concept in relation to assembled Aβ, tau, and α-synuclein. *Science* 349, 1255555–
467 1255555
468 5. Barber, R. C. (2012) The genetics of Alzheimer's disease. *Scientifica (Cairo)* 2012,
469 246210–14
470 6. Adam, M. P., Ardinger, H. H., Pagon, R. A., Wallace, S. E., Bean, L. J., Stephens, K.,
471 Amemiya, A., and Bird, T. D. (1993) Early-Onset Familial Alzheimer Disease – RETIRED
472 CHAPTER, FOR HISTORICAL REFERENCE ONLY. *PLoS Med* 14, e1002270
473 7. Bertram, L., and Tanzi, R. E. (2008) Thirty years of Alzheimer's disease genetics: the
474 implications of systematic meta-analyses. *Nat. Rev. Neurosci.* 9, 768–778
475 8. Sasaguri, H., Nilsson, P., Hashimoto, S., Nagata, K., Saito, T., De Strooper, B., Hardy, J.,
476 Vassar, R., Winblad, B., and Saido, T. C. (2017) APP mouse models for Alzheimer's disease
477 preclinical studies. *EMBO J.* 36, 2473–2487

478 9. Platt, T. L., Reeves, V. L., and Murphy, M. P. (2013) Transgenic models of Alzheimer's
479 disease: better utilization of existing models through viral transgenesis. *Biochim. Biophys. Acta*
480 1832, 1437–1448
481 10. Balducci, C., and Forloni, G. (2011) APP transgenic mice: their use and limitations.
482 *Neuromolecular Med.* 13, 117–137
483 11. Onos, K. D., Uyar, A., Keezer, K. J., Jackson, H. M., Preuss, C., Acklin, C. J., O'Rourke,
484 R., Buchanan, R., Cossette, T. L., Sukoff Rizzo, S. J., Soto, I., Carter, G. W., and Howell, G. R.
485 (2019) Enhancing face validity of mouse models of Alzheimer's disease with natural genetic
486 variation. *PLoS Genet.* 15, e1008155
487 12. Thery, C., Witwer, K. W., Aikawa, E., Alcaraz, M. J., Anderson, J. D., Andriantsitohaina,
488 R., Antoniou, A., Arab, T., Archer, F., Atkin-Smith, G. K., Ayre, D. C., Bach, J.-M., Bachurski,
489 D., Baharvand, H., Balaj, L., Baldacchino, S., Bauer, N. N., Baxter, A. A., Bebawy, M.,
490 Beckham, C., Bedina Zavec, A., Benmoussa, A., Berardi, A. C., Bergese, P., Bielska, E.,
491 Blenkiron, C., Bobis-Wozowicz, S., Boilard, E., Boireau, W., Bongiovanni, A., Borràs, F. E.,
492 Bosch, S., Boulanger, C. M., Breakefield, X., Breglio, A. M., Brennan, M. Á., Brigstock, D. R.,
493 Brisson, A., Broekman, M. L., Bromberg, J. F., Bryl-Górecka, P., Buch, S., Buck, A. H., Burger,
494 D., Busatto, S., Buschmann, D., Bussolati, B., Buzás, E. I., Byrd, J. B., Camussi, G., Carter, D.
495 R., Caruso, S., Chamley, L. W., Chang, Y.-T., Chen, C., Chen, S., Cheng, L., Chin, A. R.,
496 Clayton, A., Clerici, S. P., Cocks, A., Cocucci, E., Coffey, R. J., Cordeiro-da-Silva, A., Couch,
497 Y., Coumans, F. A., Coyle, B., Crescitelli, R., Criado, M. F., D'Souza-Schorey, C., Das, S., Datta
498 Chaudhuri, A., de Candia, P., De Santana, E. F., De Wever, O., Del Portillo, H. A., Demaret, T.,
499 Deville, S., Devitt, A., Dhondt, B., Di Vizio, D., Dieterich, L. C., Dolo, V., Dominguez Rubio,
500 A. P., Dominici, M., Dourado, M. R., Driedonks, T. A., Duarte, F. V., Duncan, H. M.,

501 Eichenberger, R. M., Ekström, K., Andaloussi, El, S., Elie-Caille, C., Erdbrügger, U., Falcon-
502 Perez, J. M., Fatima, F., Fish, J. E., Flores-Bellver, M., Försönits, A., Frelet-Barrand, A., Fricke,
503 F., Fuhrmann, G., Gabrielsson, S., Gámez-Valero, A., Gardiner, C., Gärtner, K., Gaudin, R.,
504 Gho, Y. S., Giebel, B., Gilbert, C., Gimona, M., Giusti, I., Goberdhan, D. C., Görgens, A.,
505 Gorski, S. M., Greening, D. W., Gross, J. C., Gualerzi, A., Gupta, G. N., Gustafson, D.,
506 Handberg, A., Haraszti, R. A., Harrison, P., Hegyesi, H., Hendrix, A., Hill, A. F., Hochberg, F.
507 H., Hoffmann, K. F., Holder, B., Holthofer, H., Hosseinkhani, B., Hu, G., Huang, Y., Huber, V.,
508 Hunt, S., Ibrahim, A. G.-E., Ikezu, T., Inal, J. M., Isin, M., Ivanova, A., Jackson, H. K.,
509 Jacobsen, S., Jay, S. M., Jayachandran, M., Jenster, G., Jiang, L., Johnson, S. M., Jones, J. C.,
510 Jong, A., Jovanovic-Talisman, T., Jung, S., Kalluri, R., Kano, S.-I., Kaur, S., Kawamura, Y.,
511 Keller, E. T., Khamari, D., Khomyakova, E., Khvorova, A., Kierulf, P., Kim, K. P., Kislinger, T.,
512 Klingeborn, M., Klinke, D. J., Kornek, M., Kosanović, M. M., Kovács, Á. F., Krämer-Albers, E.-
513 M., Krasemann, S., Krause, M., Kurochkin, I. V., Kusuma, G. D., Kuypers, S., Laitinen, S.,
514 Langevin, S. M., Languino, L. R., Lannigan, J., Lässer, C., Laurent, L. C., Lavieu, G., Lázaro-
515 Ibáñez, E., Le Lay, S., Lee, M.-S., Lee, Y. X. F., Lemos, D. S., Lenassi, M., Leszczynska, A., Li,
516 I. T., Liao, K., Libregts, S. F., Ligeti, E., Lim, R., Lim, S. K., Linē, A., Linnemannstöns, K.,
517 Llorente, A., Lombard, C. A., Lorenowicz, M. J., Lörincz, Á. M., Lötvall, J., Lovett, J., Lowry,
518 M. C., Loyer, X., Lu, Q., Lukomska, B., Lunavat, T. R., Maas, S. L., Malhi, H., Marcilla, A.,
519 Mariani, J., Mariscal, J., Martens-Uzunova, E. S., Martin-Jaular, L., Martinez, M. C., Martins, V.
520 R., Mathieu, M., Mathivanan, S., Maugeri, M., McGinnis, L. K., McVey, M. J., Meckes, D. G.,
521 Meehan, K. L., Mertens, I., Minciacchi, V. R., Möller, A., Møller Jørgensen, M., Morales-
522 Kastresana, A., Morhayim, J., Mullier, F., Muraca, M., Musante, L., Mussack, V., Muth, D. C.,
523 Myburgh, K. H., Najrana, T., Nawaz, M., Nazarenko, I., Nejsum, P., Neri, C., Neri, T.,

524 Nieuwland, R., Nimrichter, L., Nolan, J. P., Nolte-'t Hoen, E. N., Noren Hooten, N., O'Driscoll,
525 L., O'Grady, T., O'Loghlen, A., Ochiya, T., Olivier, M., Ortiz, A., Ortiz, L. A., Osteikoetxea, X.,
526 Østergaard, O., Ostrowski, M., Park, J., Pegtel, D. M., Peinado, H., Perut, F., Pfaffl, M. W.,
527 Phinney, D. G., Pieters, B. C., Pink, R. C., Pisetsky, D. S., Pogge von Strandmann, E.,
528 Polakovicova, I., Poon, I. K., Powell, B. H., Prada, I., Pulliam, L., Quesenberry, P., Radeghieri,
529 A., Raffai, R. L., Raimondo, S., Rak, J., Ramirez, M. I., Raposo, G., Rayyan, M. S., Regev-
530 Rudzki, N., Ricklefs, F. L., Robbins, P. D., Roberts, D. D., Rodrigues, S. C., Rohde, E., Rome,
531 S., Rouschop, K. M., Rughetti, A., Russell, A. E., Saá, P., Sahoo, S., Salas-Huenuleo, E.,
532 Sánchez, C., Saugstad, J. A., Saul, M. J., Schiffelers, R. M., Schneider, R., Schøyen, T. H., Scott,
533 A., Shahaj, E., Sharma, S., Shatnyeva, O., Shekari, F., Shelke, G. V., Shetty, A. K., Shiba, K.,
534 Siljander, P. R.-M., Silva, A. M., Skowronek, A., Snyder, O. L., Soares, R. P., Sódar, B. W.,
535 Soekmadji, C., Sotillo, J., Stahl, P. D., Stoorvogel, W., Stott, S. L., Strasser, E. F., Swift, S.,
536 Tahara, H., Tewari, M., Timms, K., Tiwari, S., Tixeira, R., Tkach, M., Toh, W. S., Tomasini, R.,
537 Torrecilhas, A. C., Tosar, J. P., Toxavidis, V., Urbanelli, L., Vader, P., van Balkom, B. W., van
538 der Grein, S. G., Van Deun, J., van Herwijnen, M. J., Van Keuren-Jensen, K., van Niel, G., van
539 Royen, M. E., van Wijnen, A. J., Vasconcelos, M. H., Vechetti, I. J., Veit, T. D., Vella, L. J.,
540 Velot, É., Verweij, F. J., Vestad, B., Viñas, J. L., Visnovitz, T., Vukman, K. V., Wahlgren, J.,
541 Watson, D. C., Wauben, M. H., Weaver, A., Webber, J. P., Weber, V., Wehman, A. M., Weiss,
542 D. J., Welsh, J. A., Wendt, S., Wheelock, A. M., Wiener, Z., Witte, L., Wolfram, J., Xagorari,
543 A., Xander, P., Xu, J., Yan, X., Yáñez-Mó, M., Yin, H., Yuana, Y., Zappulli, V., Zarubova, J.,
544 Žėkas, V., Zhang, J.-Y., Zhao, Z., Zheng, L., Zheutlin, A. R., Zickler, A. M., Zimmermann, P.,
545 Zivkovic, A. M., Zocco, D., and Zuba-Surma, E. K. (2018) Minimal information for studies of

546 extracellular vesicles 2018 (MISEV2018): a position statement of the International Society for
547 Extracellular Vesicles and update of the MISEV2014 guidelines. *J Extracell Vesicles* 7, 1535750
548 13. You, Y., and Ikezu, T. (2019) Emerging roles of extracellular vesicles in
549 neurodegenerative disorders. *Neurobiol. Dis.* 130, 104512
550 14. Delpech, J.-C., Herron, S., Botros, M. B., and Ikezu, T. (2019) Neuroimmune Crosstalk
551 through Extracellular Vesicles in Health and Disease. *Trends in Neurosciences* 42, 361–372
552 15. DeLeo, A. M., and Ikezu, T. (2018) Extracellular Vesicle Biology in Alzheimer's Disease
553 and Related Tauopathy. *J Neuroimmune Pharmacol* 13, 292–308
554 16. Guo, B. B., Bellingham, S. A., and Hill, A. F. (2016) Stimulating the Release of
555 Exosomes Increases the Intercellular Transfer of Prions. *J. Biol. Chem.* 291, 5128–5137
556 17. Dinkins, M. B., Dasgupta, S., Wang, G., Zhu, G., and Bieberich, E. (2014) Exosome
557 reduction in vivo is associated with lower amyloid plaque load in the 5XFAD mouse model of
558 Alzheimer's disease. *Neurobiol. Aging* 35, 1792–1800
559 18. Bulloj, A., Leal, M. C., Xu, H., Castaño, E. M., and Morelli, L. (2010) Insulin-degrading
560 enzyme sorting in exosomes: a secretory pathway for a key brain amyloid-beta degrading
561 protease. *J. Alzheimers Dis.* 19, 79–95
562 19. Yuyama, K., Sun, H., Mitsutake, S., and Igarashi, Y. (2012) Sphingolipid-modulated
563 exosome secretion promotes clearance of amyloid-β by microglia. *J. Biol. Chem.* 287, 10977–
564 10989
565 20. Muraoka, S., DeLeo, A. M., Sethi, M. K., Yukawa-Takamatsu, K., Yang, Z., Ko, J.,
566 Hogan, J. D., Ruan, Z., You, Y., Wang, Y., Medalla, M., Ikezu, S., Chen, M., Xia, W., Gorantla,
567 S., Gendelman, H. E., Issadore, D., Zaia, J., and Ikezu, T. (2020) Proteomic and biological

568 profiling of extracellular vesicles from Alzheimer's disease human brain tissues. *Alzheimers*
569 *Dement* 16, 896–907
570 21. Muraoka, S., Lin, W., Chen, M., Hersh, S. W., Emili, A., Xia, W., and Ikezu, T. (2020)
571 Assessment of separation methods for extracellular vesicles from human and mouse brain tissues
572 and human cerebrospinal fluids. *Methods*,
573 22. McAlister, G. C., Nusinow, D. P., Jedrychowski, M. P., Wühr, M., Huttlin, E. L.,
574 Erickson, B. K., Rad, R., Haas, W., and Gygi, S. P. (2014) MultiNotch MS3 enables accurate,
575 sensitive, and multiplexed detection of differential expression across cancer cell line proteomes.
576 *Anal. Chem.* 86, 7150–7158
577 23. Elias, J. E., and Gygi, S. P. (2007) Target-decoy search strategy for increased confidence
578 in large-scale protein identifications by mass spectrometry. *Nat. Methods* 4, 207–214
579 24. Huttlin, E. L., Jedrychowski, M. P., Elias, J. E., Goswami, T., Rad, R., Beausoleil, S. A.,
580 Villén, J., Haas, W., Sowa, M. E., and Gygi, S. P. (2010) A tissue-specific atlas of mouse protein
581 phosphorylation and expression. *Cell* 143, 1174–1189
582 25. Ting, L., Rad, R., Gygi, S. P., and Haas, W. (2011) MS3 eliminates ratio distortion in
583 isobaric multiplexed quantitative proteomics. *Nat. Methods* 8, 937–940
584 26. Perez-Riverol, Y., Csordas, A., Bai, J., Bernal-Llinares, M., Hewapathirana, S., Kundu,
585 D. J., Inuganti, A., Griss, J., Mayer, G., Eisenacher, M., Pérez, E., Uszkoreit, J., Pfeuffer, J.,
586 Sachsenberg, T., Yilmaz, S., Tiwary, S., Cox, J., Audain, E., Walzer, M., Jarnuczak, A. F.,
587 Ternent, T., Brazma, A., and Vizcaíno, J. A. (2019) The PRIDE database and related tools and
588 resources in 2019: improving support for quantification data. *Nucleic Acids Res.* 47, D442–D450

589 27. Paulo, J. A., Jedrychowski, M. P., Chouchani, E. T., Kazak, L., and Gygi, S. P. (2018)
590 Multiplexed Isobaric Tag-Based Profiling of Seven Murine Tissues Following In Vivo Nicotine
591 Treatment Using a Minimalistic Proteomics Strategy. *Proteomics* 18, e1700326
592 28. Keerthikumar, S., Chisanga, D., Ariyaratne, D., Saffar, Al, H., Anand, S., Zhao, K.,
593 Samuel, M., Pathan, M., Jois, M., Chilamkurti, N., Gangoda, L., and Mathivanan, S. (2016)
594 ExoCarta: A Web-Based Compendium of Exosomal Cargo. *J. Mol. Biol.* 428, 688–692
595 29. Huang, D. W., Sherman, B. T., and Lempicki, R. A. (2009) Systematic and integrative
596 analysis of large gene lists using DAVID bioinformatics resources. *Nat Protoc* 4, 44–57
597 30. Dennis, G., Sherman, B. T., Hosack, D. A., Yang, J., Gao, W., Lane, H. C., and
598 Lempicki, R. A. (2003) DAVID: Database for Annotation, Visualization, and Integrated
599 Discovery. *Genome Biol.* 4, P3
600 31. Sharma, K., Schmitt, S., Bergner, C. G., Tyanova, S., Kannaiyan, N., Manrique-Hoyos,
601 N., Kongi, K., Cantuti, L., Hanisch, U.-K., Philips, M.-A., Rossner, M. J., Mann, M., and
602 Simons, M. (2015) Cell type- and brain region-resolved mouse brain proteome. *Nat. Neurosci.*
603 18, 1819–1831
604 32. Keren-Shaul, H., Spinrad, A., Weiner, A., Matcovitch-Natan, O., Dvir-Szternfeld, R.,
605 Ulland, T. K., David, E., Baruch, K., Lara-Astaiso, D., Toth, B., Itzkovitz, S., Colonna, M.,
606 Schwartz, M., and Amit, I. (2017) A Unique Microglia Type Associated with Restricting
607 Development of Alzheimer's Disease. *Cell* 169, 1276–1290.e17
608 33. Krasemann, S., Madore, C., Cialic, R., Baufeld, C., Calcagno, N., Fatimy, El, R.,
609 Beckers, L., O'Loughlin, E., Xu, Y., Fanek, Z., Greco, D. J., Smith, S. T., Tweet, G., Humulock,
610 Z., Zrzavy, T., Conde-Sanroman, P., Gacias, M., Weng, Z., Chen, H., Tjon, E., Mazaheri, F.,
611 Hartmann, K., Madi, A., Ulrich, J. D., Glatzel, M., Worthmann, A., Heeren, J., Budnik, B.,

612 Lemere, C., Ikezu, T., Heppner, F. L., Litvak, V., Holtzman, D. M., Lassmann, H., Weiner, H.
613 L., Ochando, J., Haass, C., and Butovsky, O. (2017) The TREM2-APOE Pathway Drives the
614 Transcriptional Phenotype of Dysfunctional Microglia in Neurodegenerative Diseases. *Immunity*
615 47, 566–581.e9
616 34. Clayton, K. A., Van Enoo, A. A., and Ikezu, T. (2017) Alzheimer's Disease: The Role of
617 Microglia in Brain Homeostasis and Proteopathy. *Front Neurosci* 11, 680
618 35. Vermes, I., Haanen, C., Steffens-Nakken, H., and Reutelingsperger, C. (1995) A novel
619 assay for apoptosis. Flow cytometric detection of phosphatidylserine expression on early
620 apoptotic cells using fluorescein labelled Annexin V. *J. Immunol. Methods* 184, 39–51
621 36. Benmamar-Badel, A., Owens, T., and Wlodarczyk, A. (2020) Protective Microglial
622 Subset in Development, Aging, and Disease: Lessons From Transcriptomic Studies. *Front*
623 *Immunol* 11, 430
624 37. Orre, M., Kamphuis, W., Osborn, L. M., Jansen, A. H. P., Kooijman, L., Bossers, K., and
625 Hol, E. M. (2014) Isolation of glia from Alzheimer's mice reveals inflammation and dysfunction.
626 *Neurobiol. Aging* 35, 2746–2760
627 38. Clayton, K. A., Delpech, J.-C., Herron, S., Iwahara, N., Saito, T., Saido, T. C., Ikezu, S.,
628 and Ikezu, T. (2020) Amyloid plaque deposition accelerates tau propagation via activation of
629 microglia in a humanized APP mouse model. *bioRxiv* 11, 2020.09.22.308015
630

631 **Table 1**

Protein Id	Gene Symbol	WT average	*APP/PS1* average	fold change	-log$_{10}$(*p*-value)[a]
E9Q2W9	Actn4	34.11	20.29	0.59	1.562
Q9ERF3	Wdr61	32.77	20.62	0.63	2.349
Q9EST5	Anp32b	47.50	23.84	0.50	1.812
Q9DC61	Pmpca	28.57	11.91	0.42	2.019
Q9JIZ0	Cml1	45.26	33.66	0.74	1.311
P46735	Myo1b	181.70	146.27	0.81	2.917
E9Q137	Tex264	167.37	123.23	0.74	1.527
Q62148	Aldh1a2	237.12	148.74	0.63	1.996
Q9D6J6	Ndufv2	575.30	330.89	0.58	1.413
Q8C5H8	Nadk2	153.93	131.47	0.85	1.324
P16254	Srp14	159.83	111.25	0.70	1.794
O35887	Calu	596.76	394.05	0.66	1.892
P24472	Gsta4	260.99	200.33	0.77	1.753
Q9CQN1	Trap1	131.26	98.76	0.75	1.512
Q05920	Pc	944.43	818.06	0.87	1.658
Q8BIP0	Dars2	27.08	18.13	0.67	1.895
Q6ZQK5	Acap2	811.17	944.92	1.16	1.452
P62242	Rps8	647.87	897.33	1.39	1.536
P62301	Rps13	600.46	848.51	1.41	1.364
Q8BT60	Cpne3	1068.06	1156.14	1.08	1.351
P39447	Tjp1	124.75	156.82	1.26	1.990
Q61730	Il1rap	1109.54	1283.78	1.16	1.371
P48036	Anxa5	2756.53	3220.07	1.17	1.693
Q921E2	Rab31	93.36	121.57	1.30	1.387
P14824	Anxa6	3667.05	4291.27	1.17	1.467
P58021	Tm9sf2	321.28	416.33	1.30	1.364
P05067-4	APP	1441.70	3198.42	2.22	2.850
P49768	PSEN1	229.33	382.95	1.67	4.245
Q91VU0	Fam3c	103.78	141.34	1.36	1.439
Q99PD7	Slc24a3	59.07	79.27	1.34	1.524
Q9CQJ6	Denr	26.78	36.86	1.38	1.710
Q9JJC6	Rilpl1	22.97	30.63	1.33	1.476
Q80TL7	Mon2	103.59	129.03	1.25	1.681
Q3B7Z2	Osbp	370.13	474.24	1.28	1.308
Q9QXH4	Itgax	29.00	78.77	2.72	2.291
Q8C7N7	Aph1b	69.45	102.88	1.48	1.993
P06800	Ptprc	143.06	210.96	1.47	1.636
P20491	Fcer1g	86.16	127.79	1.48	1.455
Q9CPV9	P2ry12	2248.44	2808.41	1.25	1.613
P60766	Cdc42	844.66	932.37	1.10	0.370
Q80UP3	Dgkz	167.80	207.27	1.24	1.670
P62192	Psmc1	1531.69	1674.17	1.09	1.746
Q5SYD0	Myo1d	1717.22	2076.67	1.21	1.350
A2ADY9	Ddi2	84.14	104.29	1.24	2.941
A2AF47	Dock11	198.13	296.61	1.50	1.329
Q8BIK4-2	Dock9	725.87	1049.00	1.45	1.415

632 [a]The t.test was calculated by Welch's test.
633
634
635

636

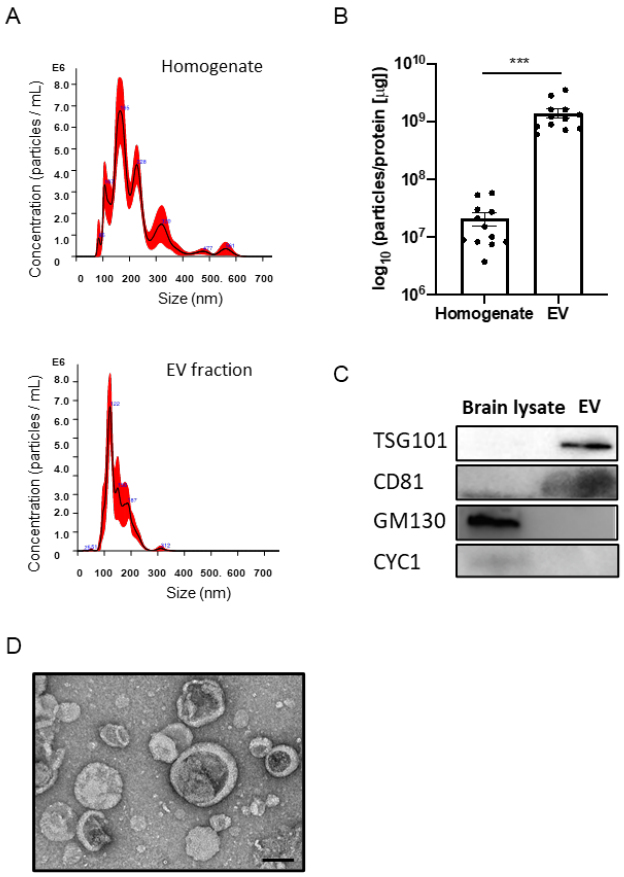

Figure 1. Biochemical characteristic of brain-derived EVs separated from frozen mouse brain tissue: A) NTA plot of average size and concentration of particles from brain homogenates and separated EV fraction. The black line shows the fitting curve. Red line represents the error bar. The y axis is the concentration of particles. The x axis is the size of particle. Top: brain homogenates, Bottom: separated EV fraction. **B)** The ratio of particles to protein concentration to quantify particle purity ($p = 0.005$ by paired samples Wilcoxon test). **C)** Assessment of EV and non-EV marker protein, including TSG101, CD81, GM130 (Golgi marker), CYC1 (Mitochondrial marker) in separated EV fraction. **D)** Transmission electron microscopy (TEM) image of mouse brain-derived EV fraction. Scale bar; 100 nm.

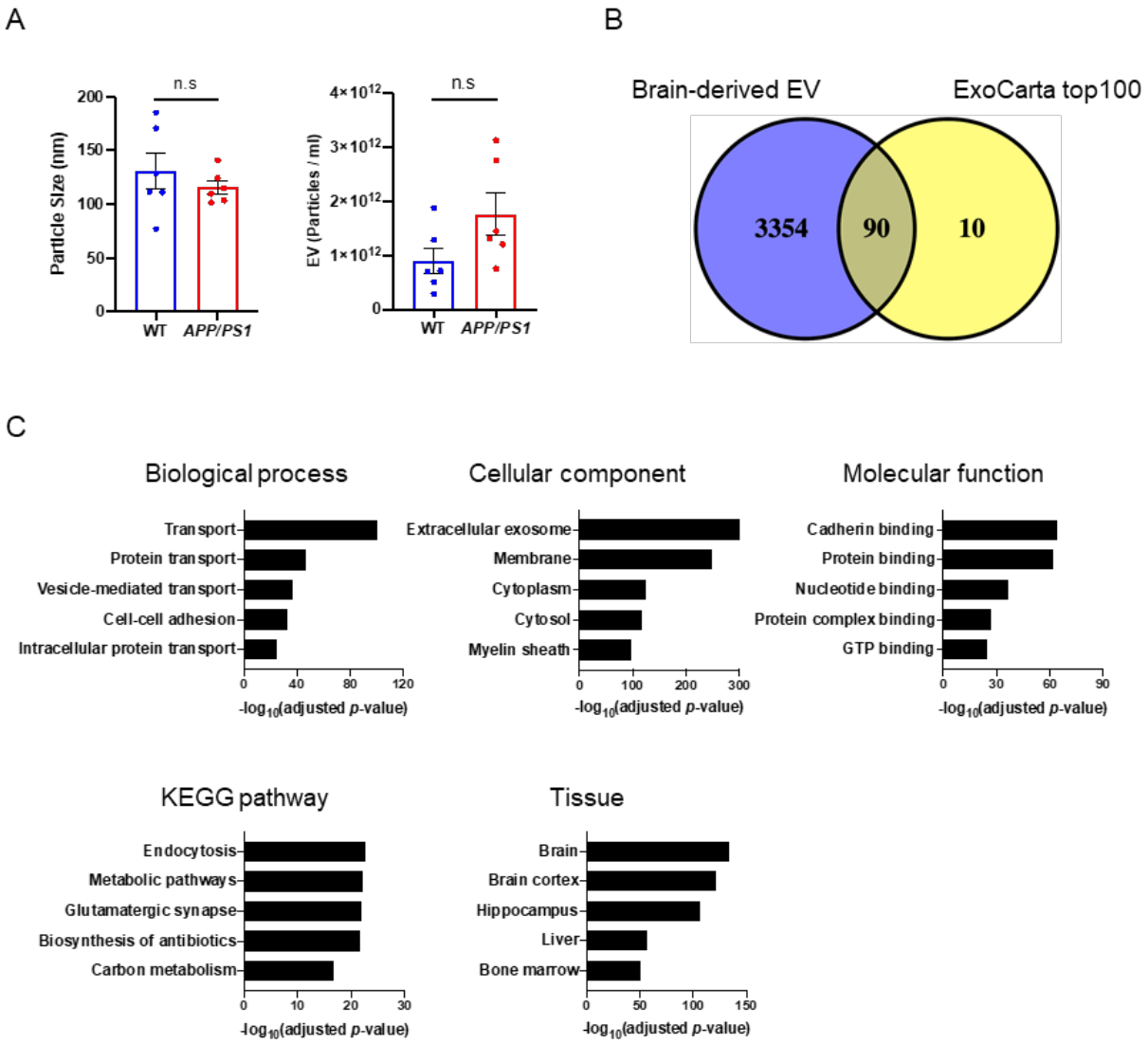

647

648 **Figure 2. Proteomic profiling of mouse brain-derived EV: A)** Comparison of particle number

649 and size in EV fraction separated from CAST.*APP/PS1* and WT mouse brain tissue. Left:

650 particle size, Right: particle number. **B)** Venn diagram representing the proteins identified in

651 brain-derived EV and ExoCarta top100. **C)** DAVID GO analysis using DAVID Bioinformatics

652 Resources 6.8. The GO term of Top5 Biological Process, Cellular Component, Molecular

653 Function, KEGG pathway and Tissue ontology with -$\log_{10}$ (FDR *p*-value).

654

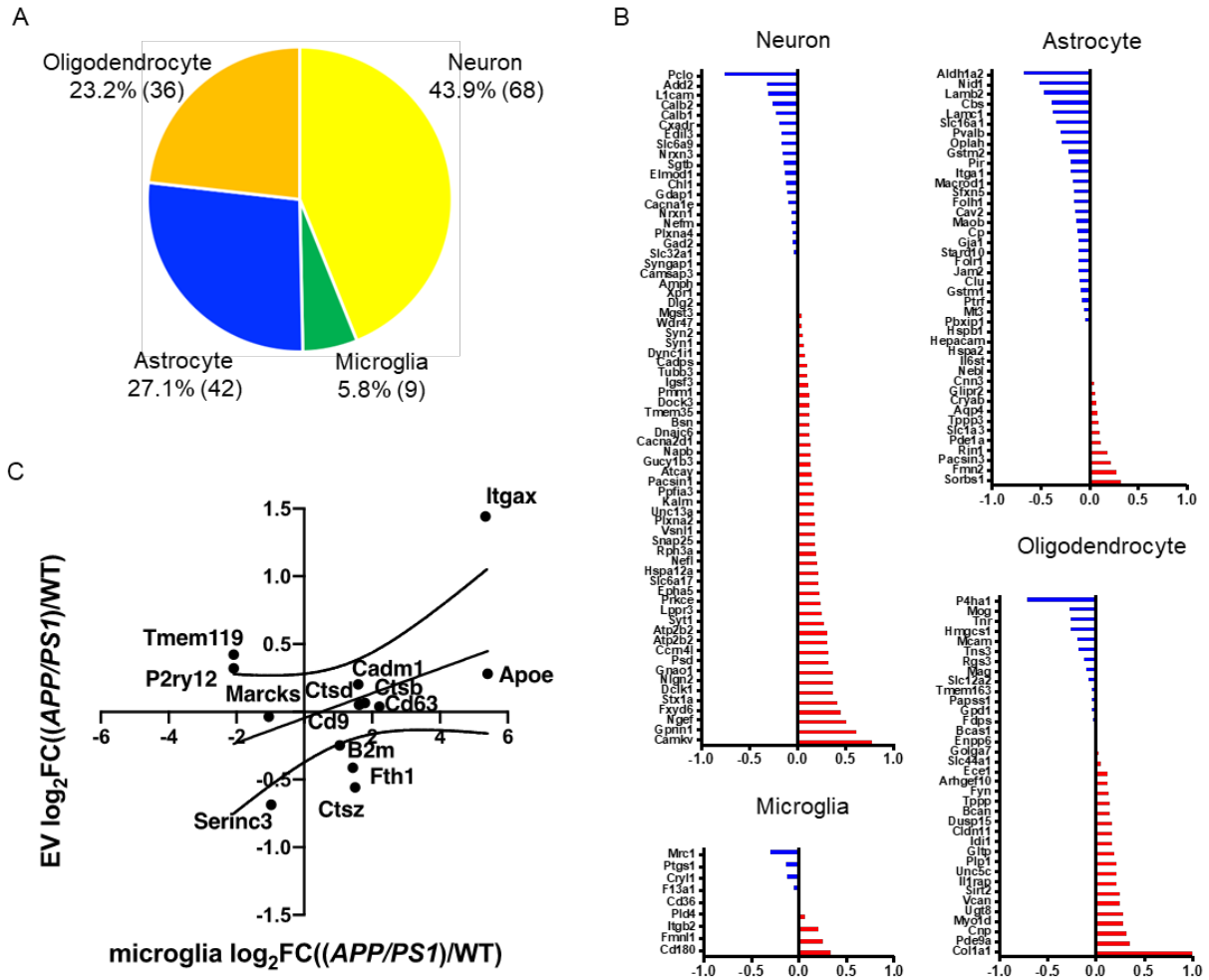

Figure 3. Cell type-specific proteins comparison of CAST. *APP/PS1* and WT mouse brain-derived EV: A) Enrichment of brain cell type-specific markers in brain-derived EV proteins. Yellow: Neuron, Green: Microglia, Blue: Astrocytes, Orange: Oligodendrocytes. The parentheses show the number of identified cell type-specific proteins. **B)** Comparison of the cell type-specific protein in CAST.*APP/PS1*-derived EVs and CAST WT EVs. The red bar shows higher expression in *APP/PS1* compared with WT and Blue bar indicates higher expression in WT compared with *APP/PS1*. **C)** Comparison of $\log_2$ fold change of the differential expression of DAM versus homeostatic microglia in the 5xFAD (x axis) to the $\log_2$ fold change of the differential expression of CAST.*APP/PS1* versus WT (y axis).

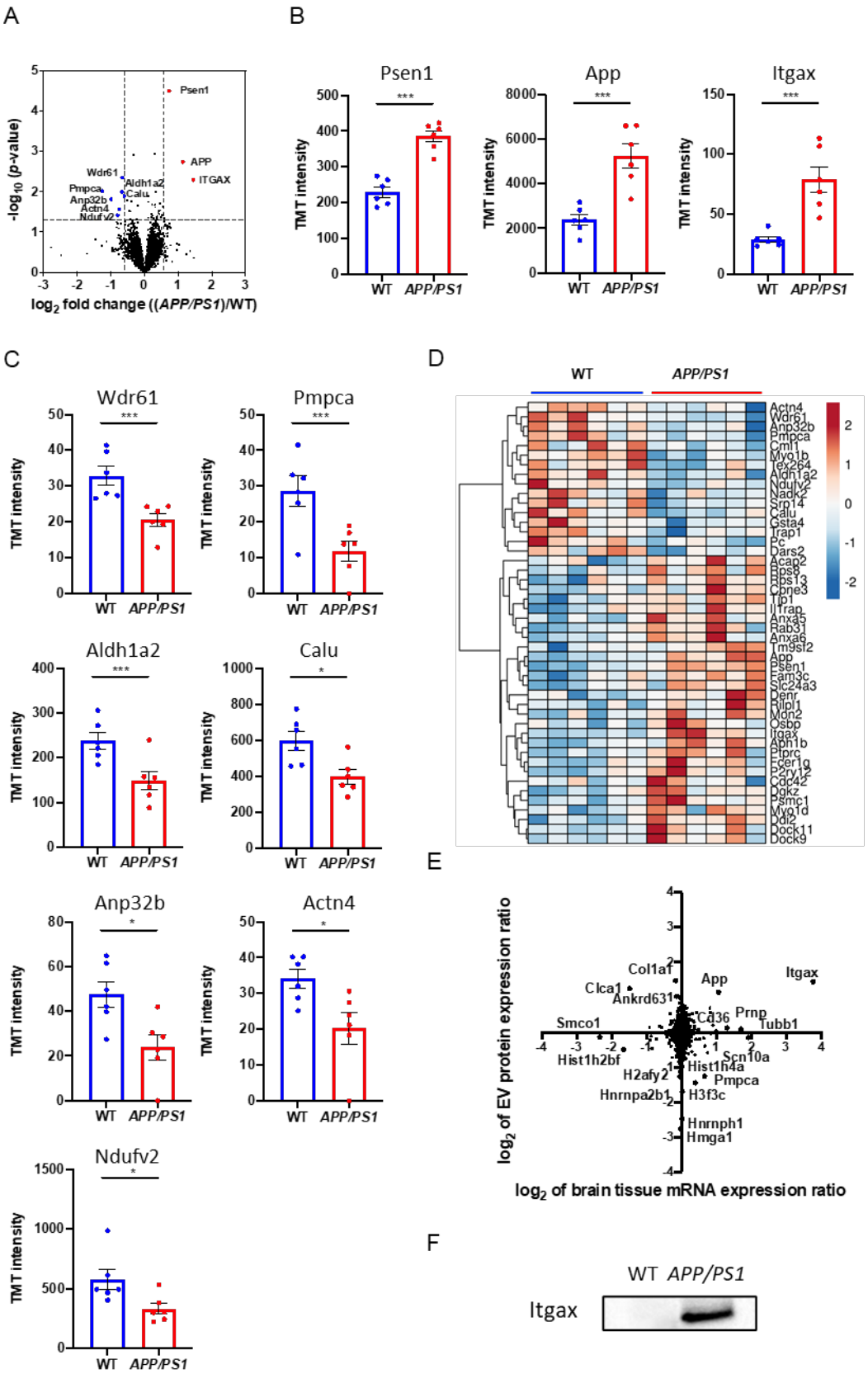
A
B
C
D
E
F
Psen1
APP
ITGAX
Wdr61
Aldh1a2
Calu
Pmpca
Anp32b
Actn4
Ndufv2
-log10 (p-value)
log2 fold change ((APP/PS1)/WT)
TMT intensity
WT
APP/PS1
***
*
Col1a1
Clca1
Ankrd631
Smco1
Hist1h2bf
H2afy2
Hnrnpa2b1
Hnrnph1
Hmga1
Hist1h4a
H3f3c
Scn10a
Cd36
Prnp
Tubb1
Itgax
log2 of EV protein expression ratio
log2 of brain tissue mRNA expression ratio
Itgax

665

666 **Figure 4. Comparison of CAST.*APP/PS1* brain-derived EV and CAST WT EV: A)** Volcano
667 plot showing degree of differential expression of brain-derived EV proteins in AAP/PS1
668 compared with WT. The x-axis indicates $\log_2$ transformed fold change in expression. The y-axis
669 shows $-\log_{10}$ transformed *p*-values. The grey dot line shows the 1.3010 $-\log_{10}$(*p*-value) cutoff and
670 0.585 or -0.585 $\log_2$FC cutoff. **B, C)** A scatter plot of TMT reporter ion intensity as measured by
671 proteomics per selected candidate protein. The t.test was calculated by Welch's test. **B)** The three
672 proteins were up-regulated in *APP/PS1* compared to WT. Psen1: $-\log_{10}$(*p*-value) = 4.245, FC =
673 1.67, App: $-\log_{10}$(*p*-value) = 2.850, FC = 2.22, Itgax: $-\log_{10}$(*p*-value) = 2.291, FC = 2.72. **C)** The
674 7 proteins were down-regulated in *APP/PS1* compared to WT. Wdr61: $-\log_{10}$(*p*-value) = 2.349,
675 FC = 0.63, Pmpca: $-\log_{10}$(*p*-value) = 2.019, FC = 0.42, Aldh1a2: $-\log_{10}$(*p*-value) = 1.996, FC =
676 0.63, Calu: $-\log_{10}$(*p*-value) = 1.892, FC = 0.66, Anp32b: $-\log_{10}$(*p*-value) = 1.812, FC = 0.50,
677 Actn4: $-\log_{10}$(*p*-value) = 1.562, FC = 0.59 and Ndufv2: $-\log_{10}$(*p*-value) = 1.413, FC = 0.58. **D)**
678 Heatmap of 46 proteins with the 1.3010 $-\log_{10}$(*p*-value) cutoff. The value shows $\log_2$(FC). **E)**
679 Comparison of protein expression and mRNA expression in *APP/PS1* and WT. The y axis is the
680 ratio of EV protein expression. The x axis is the ratio of brain tissue mRNA expression. The
681 Spearman rank correlation coefficient (rho) shows 0.06709 ($p = 0.0001$). F) Validation of Itgax
682 in separated EV fraction from CAST.*APP/PS1* and WT mouse brain tissue using Western blot.